Hindawi
Advances in Materials Science and Engineering
Volume 2022, Article ID 7040685, 12 pages
https://doi.org/10.1155/2022/7040685

Research Article

Study on the Thermal Conductivity of Cu/Al Joints with Different Interfacial Microstructures

Yanni Wei,[1,2] **Yu Chen**,[1] **Rui Niu**,[1] **Qing Yang**,[1,2] **Yongguang Luo**,[3] **and Juntao Zou**[1,2]

[1]*Department of Materials Science and Engineering, Xi'an University of Technology, 5 South Jinhua Road, Xi'an 710048, China*
[2]*Shaanxi Province Key Laboratory for Electrical Materials and Infiltration Technology, Xi'an University of Technology, Xi'an, Shaanxi 710048, China*
[3]*Yunnan Chihong Zn & Ge Co., Ltd, Qujing, Yunnan 655011, China*

Correspondence should be addressed to Yanni Wei; weiyanni@xaut.edu.cn

Received 11 August 2021; Revised 30 January 2022; Accepted 17 February 2022; Published 11 March 2022

Academic Editor: Dimitrios E. Manolakos

Three types of Cu/Al joints with different interfacial microstructures prepared by diffusion bonding, friction stir welding, and explosive welding were obtained, and the interfacial thermal conductivity was emphatically discussed in this paper. Two layers of intermetallic compounds with a width of 5~12 μm were formed in the joint prepared by diffusion bonding. And a mixture of a supersaturated solid solution and few dispersed compounds with a thickness less than 1 μm was formed in the friction stir welding Cu/Al joint. The bonding interface of the Cu/Al explosive welding joint presented a wavy-like morphology with a width of 300~350 μm. The interfacial thermal conductivity with different interfacial microstructure was calculated analytically using the acoustic mismatch model and compared with the measured value of the joints. The interfacial thermal conductivity mainly depends on the type of interfacial phase and its thickness. The calculated result showed that the interfacial thermal conductivity of friction stir welding joint was the highest ($1\sim8\times10^7$ W m^{-2}·K^{-1}). The experiment results suggested that the interfacial thermal conductivity showed the trend that explosive welding < friction stir welding < diffusion bonding.

1. Introduction

As a typical thermal/electrical component, Cu/Al hybrid structures have been widely used in industries such as circuit transmission, heat dissipation, shipbuilding, hydrometallurgy, and other fields [1–3]. For example, copper cladding aluminum used in a wire can not only reduce the quality of the wire by 50% but also greatly reduce the cost of the wire by 35% under the same conductivity condition [4]. Cu/Al hybrid plate radiator can realize the effective combination of thermal conductivity and heat dissipation, and improve the cost performance [5]. All of these Cu/Al structures are related to the Cu/Al heterogeneous joining. And the interfacial microstructure and performance play a key role in the service efficiency and service life of the Cu/Al hybrid structure [6, 7].

However, it is difficult to obtain a satisfactory Cu/Al joint due to the significant difference in metallurgical and chemical properties. Meanwhile, the brittle intermetallic compounds (IMCs) are easily formed, which seriously deteriorates the mechanical properties and the conductivity of the Al/Cu joints [8, 9]. In the present study, different welding methods, in case of diffusion bonding (DB) [10], brazing [11, 12], friction stir welding (FSW) [13–15], laser welding [16], and explosion welding (EW) [17, 18], have been proved to be an alternative method in joining Al and Cu. These studies have shown that it was inevitable to form the hard and brittle Al_xCu_y phases such as Al_2Cu, AlCu, Al_4Cu_9, and Al_3Cu_4 on the interface of Cu/Al joints. These IMCs promoted creak propagation and weakened the joint [19]. Wang et al. [20] found the formation of Al_2Cu and voids in the Al/Cu joint during the diffusion brazing. Tavassoli et al. [21] found that the thermal conductivity and joint strength decreased with the increase of total thickness of IMCs. Tanaka et al. [22] found that the joint strength was inversely proportional to the IMC thickness. All the above

investigations verified that the interfacial microstructure (including thickness, phase type, and distribution) had important effects on the properties of the Cu/Al joint. The influence of the preparation technology and the interfacial microstructure on the joint strength has been studied extensively [13, 23, 24]. Less attention has been paid to the interfacial thermal conductivity of the Cu/Al heterogeneous interface area. However, the interfacial thermal resistance not only seriously affects the thermal conductivity of the joint but also has great influence on the service life when it is used as a conductive component. It has great practical significance to study the interfacial thermal conductivity of Cu/Al joint and reveal the thermal conductivity mechanism of Cu/Al heterogeneous interface with different interface structures.

In this paper, three types of Cu/Al joints with different interfacial microstructures prepared by DB, FSW, and EW were obtained and evaluated. The microstructures and compositions of the Cu/Al joints were investigated. The thermal conductivity was estimated, and the corresponding interface thermal conductivity model was built. The influence of different interface structures and thicknesses on the thermal conductivity of Cu/Al joints was analyzed.

2. Experimental Details

Considering that Cu/Al structures are mostly used as conductive and thermal components, 1060 Al (99.6 wt%) and T2 Cu (99.9 wt%) were selected as the base metals. Table 1 shows the composition and properties. DB, FSW, and EW were used to fabricate Cu/Al joints in this study. The microstructure and thermal conductivity properties of Cu/Al joints with different interface structures obtained by three methods are emphatically discussed.

For the Cu/Al vacuum DB process, after ultrasonic cleaning and drying, the specimens were put into the furnace for assembly. The bonding process proceeded at 565°C for 30 min and 60 min in a vacuum furnace ($3.0\sim5.0\times10^{-3}$ Pa). The welding pressure was maintained at 5 MPa during the welding process. The details of the parameters optimized are in the previous work [25]. FSW of the Cu/Al plates was conducted using a XA5032 vertical milling machine. Preliminary experiments showed that no surface defect joint can be obtained when Cu was fixed on the advancing side [15]. In the FSW process, the homemade fixtures were used. And a single-pass but mode was used. The Cu plate was placed on the advancing side and the Al plate placed on the retreating side. The welding speed was selected as 60 mm/min, and the rotation speed was in the range of 750~1500 rpm, which could obtain the appropriate heat input. The welding process proceeded at the welding speed of 60 mm/min and the rotation speed of 1180 and 950 rpm in this paper. The Cu/Al EW joints were prepared by Xi'an Tianli Clad Metal Materials Co., Ltd. The Cu and Al plates were assembled in parallel as the flying and base plates. Detailed parameter description of the EW process is presented in reference [26]. The stand-off distance was 1.35 mm, the explosive ratio of 2.1, the detonation velocity was 2100 m/s, and the impact velocity V_p was 851 m/s [26]. Figure 1 shows the experimental schematic diagram of the DB, FSW, and EW processes. Cu/Al interface with different interfacial microstructures and thicknesses can be obtained by different methods.

After welding, the samples were cut perpendicular to the welding interface. All samples were subjected to metallographic characterization by the scanning electron microscopy (SEM, JEOL, JSM-6700) with an energy-dispersive spectrum (EDS). The phase composition of the fracture surfaces was investigated by an X-ray diffraction (XRD) instrument with Cu Ka radiation. The joint welding strength was evaluated by shear tests with the Instron 5880 machine. The microhardness of the Cu/Al joint was measured using the TUKON2100 Vickers microhardness tester with the loading of 10 g and the dwell time of 10 s. The thermal conductivity of the Cu/Al composite combined layer was measured using the Xenon lamp thermal conductivity meter DXF200 (TA Instruments, USA). Combining the layer into the cylinder, the specification was Ø12.7 mm × 1 mm and the experiment temperature was 30°C.

3. Results and Discussion

3.1. Microstructure of the Cu/Al Bonded Interface

3.1.1. Interface Microstructure of Vacuum DB Cu-Al Joint. Figure 2 shows the microstructure of the Cu/Al joints with different holding times during the DB process. Two layers of products with different grayscales were formed on Cu/Al interface when the holding time was 30 min, and three layers were formed on the joint when the holding time was 60 min. The total width of the diffusion reaction layer in the interface region was in the range of 5~12 μm. The layer near the Cu side was continuous laminar, and the layer near the Al side shows an uneven bump on the contact interface with the Al base metal. With the increase of holding time, the thickness of the diffusion interaction layer has significantly increased.

Figure 3 shows the analysis of the elemental composition and phase composition of the Cu/Al interface region. The distribution of elements perpendicular to the interface is shown in Figure 3(a). EDS spot scan analysis was used to preliminarily determine the compound. The spectrograms and the element content of the different regions indicated in Figure 2 are shown in Figures 3(c)–3(e). The EDS analysis of point 02 in Figure 2(b) and point 05 in Figure 2(d) suggested that these were possible Al4Cu9 phases. The EDS analysis of point 01 in Figure 2(b) and point 03 in Figure 2(d) located layer near the Al side showed that the atom ratio of Al : Cu was close to 2 : 1. It could be speculated as the Al_2Cu phase. A layer appears between Al_4Cu_9 and Al_2Cu layers when the holding time is extended to 60 min. It has a gray scale similar to the Al_4Cu_9 phase, and EDS data showed that it was the AlCu phase, as shown in Figure 3(d).

In order to further determine the phase on the Al/Cu interface of the joints prepared by vacuum DB, XRD analyses were carried out on the fracture surface. The fracture morphology showed that a part of the fracture

Table 1: Composition and properties of 1060 Al and T2 Cu base metals used in this paper.

Base metal	Composition (mass %)	Melting point (°C)	Coefficient of linear expansion ($10^{-6}K^{-1}$)	Heat conductivity/ $W(m{\cdot}K)^{-1}$	Tensile strength (MPa)	Resistivity ($10^{-9}\Omega{\cdot}m$)
1060 Al	Al ≥ 99.6%	1083	16.5	394.0	83~91	27.6~29.1
T2 Cu	Cu ≥ 99.9%	660	23.6	222.0	293~300	17.1~18.5

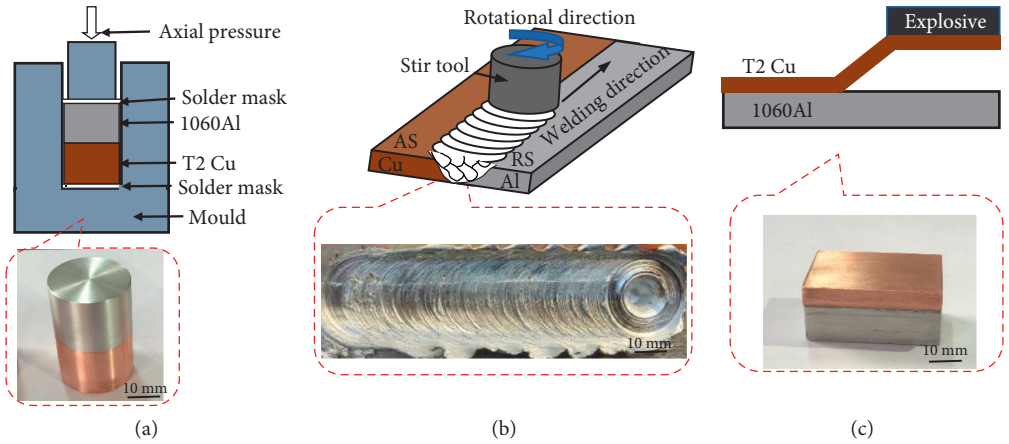

Figure 1: The experimental schematic diagram. (a) DB, (b) FSW, and (c) EW.

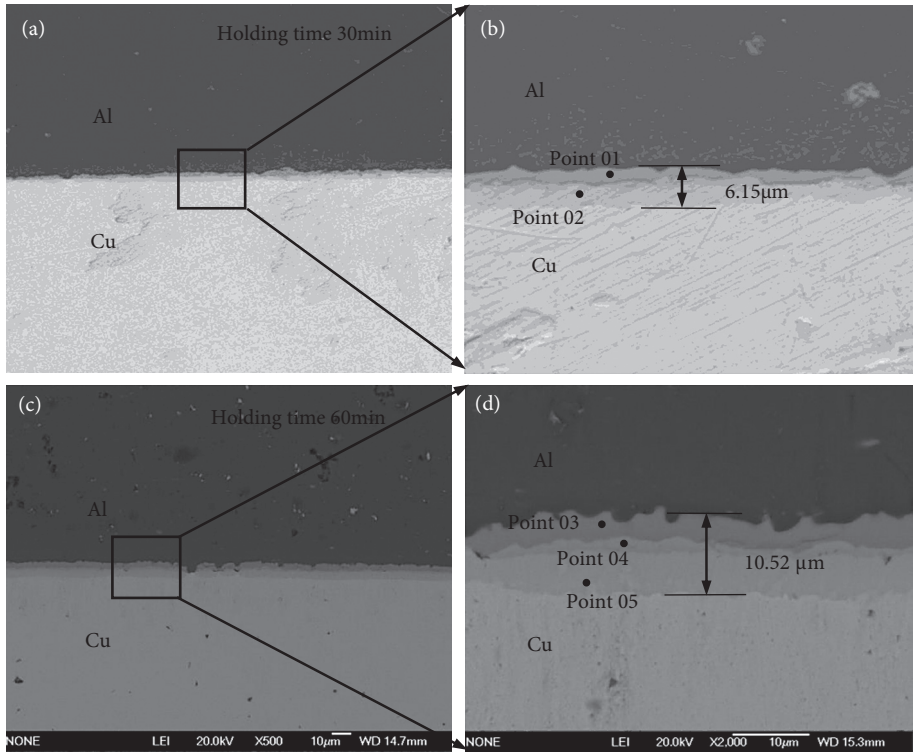

Figure 2: The microstructure of the Cu/Al joints with different holding time. (a, b) 30 min and (c, d) 60 min.

occurred at the interface of the two compounds and a part occurred inside the compound [25]. The results are shown in Figure 3(b). The diffraction peak of Al_2Cu and Al_4Cu_9 was found in both joints, which are consistent with the above point scanning results. There was no obvious diffraction peak of the AlCu phase. This may be

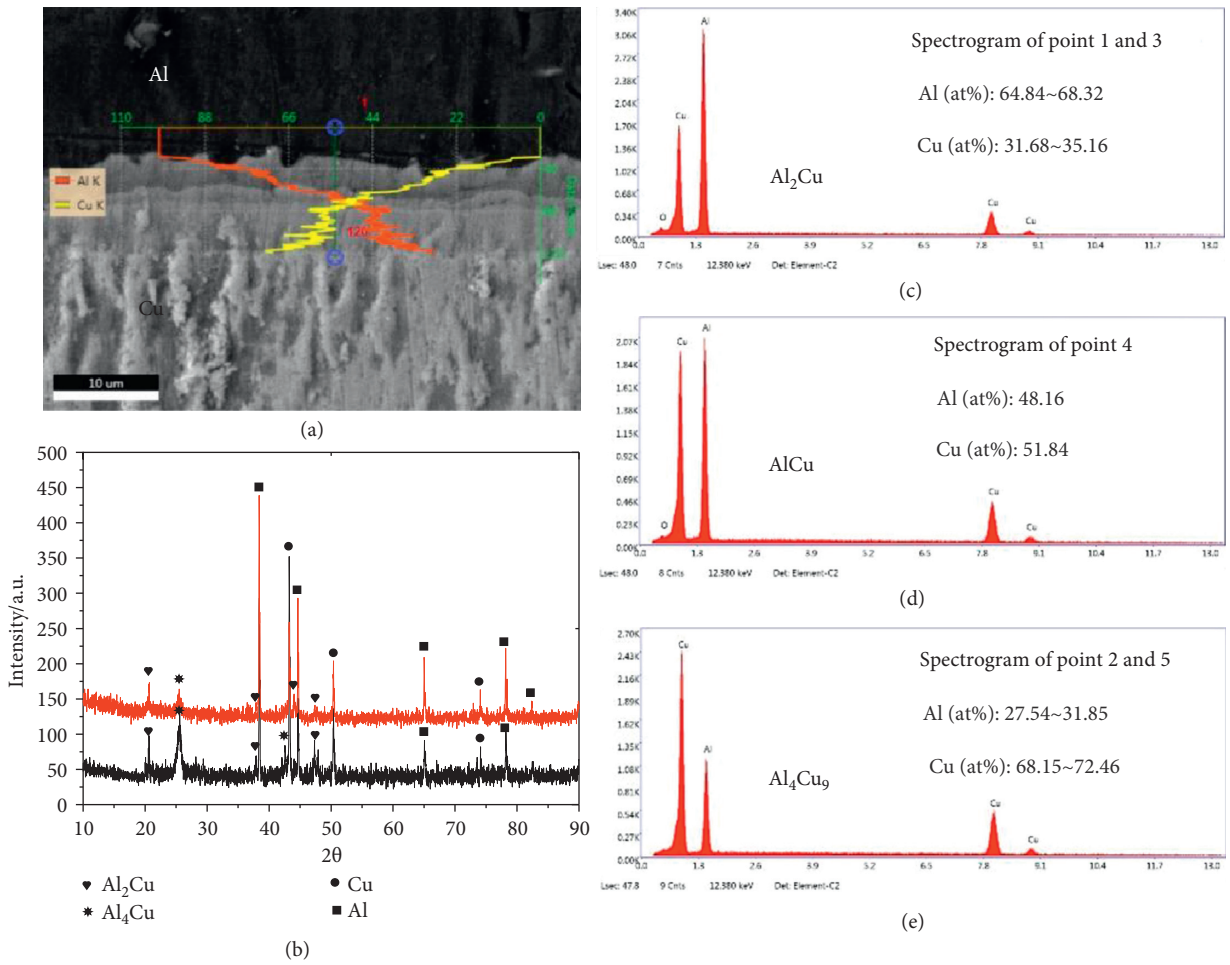

Figure 3: Analysis of elemental composition and phase composition of the joint prepared by DB. (a) Element distribution perpendicular to the interface, (b) XRD analysis results of the fracture surface, and (c–e) spectrograms and element contents.

due to the small amount of the Al/Cu phase, which cannot cause an obvious diffraction peak. In addition, it is also related to the fracture location.

3.1.2. Interface Microstructure of FSW Cu/Al Joint. The microstructure of the interfacial region of the Cu/Al FSW joint produced by different rotation speed is shown in Figure 4. The metallurgical reaction occurred during the FSW process. An obvious diffusion layer with the thickness less than 1 μm was formed on the Cu/Al interface. EDS spot scan analysis and XRD analyses on the fracture surface were all carried out to determine the compound on the interface. The related results are shown in Figure 5. The chemical composition changed gradually from the Al side to the Cu side. It indicated that there were no obvious IMCs of fixed composition formed. The XRD pattern showed a weak Al_2Cu diffraction peak on the fracture surface. It indicated that a small number of Al_2Cu phases were formed. But there is no continuous lamellar formation. In addition, there were some particles distributed in the aluminum side matrix.

The formation mechanism of these particles was discussed in detail in reference [15].

3.1.3. Interface Microstructure of EW Cu/Al Joint. Figure 6 shows the microstructure of the Cu/Al joint produced by EW. The bonding interface presented a wavy-like morphology. An enlarged vortex structure is shown in Figure 6(b). Different interface morphologies were analyzed with an enlarge view of region A and B indicated by the blue dotted circle in Figure 6(b). In the region A, it presented good bonding with a transition layer of 5 μm. There were some light gray needle-like structures embedded in a dark gray substrate in this region, as shown in Figure 6(c). The EDS analysis showed that the light gray needle-like structures were the Cu-rich solid solution and the dark gray substrate near Al side was the Al-rich solid solution. The spectrograms are shown in Figure 7. In the region B, a vortex structure was formed and defects such as pores and cracks were appeared. A large number of brittle IMCs were generated. The thickness was approximately 300~350 μm. The atom ratio of the point 08 and 09 indicated that compounds in the vortex region were possible Al_2Cu phases. XRD analysis further confirmed the existence of the Al_2Cu phase.

3.2. Mechanical Properties of Cu/Al Joints. The shear strength and the microhardness of three types of Cu/Al joints were tested. The test results are shown in Figure 8. In the shear

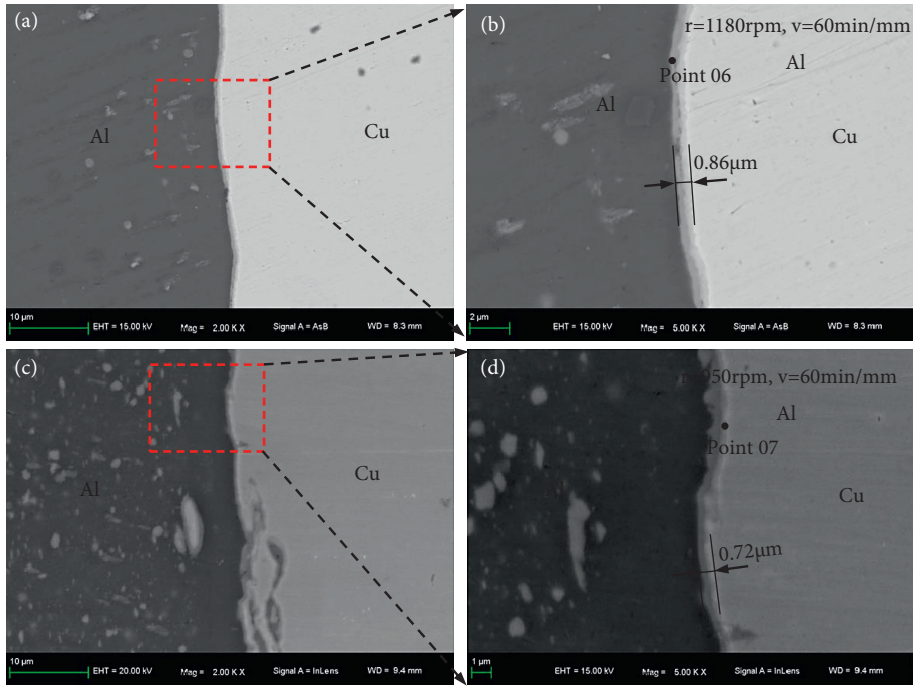

Figure 4: The microstructure of the FSW Cu/Al joints with different rotation speed. (a, b) 1180 rpm and (c, d) 950 rpm.

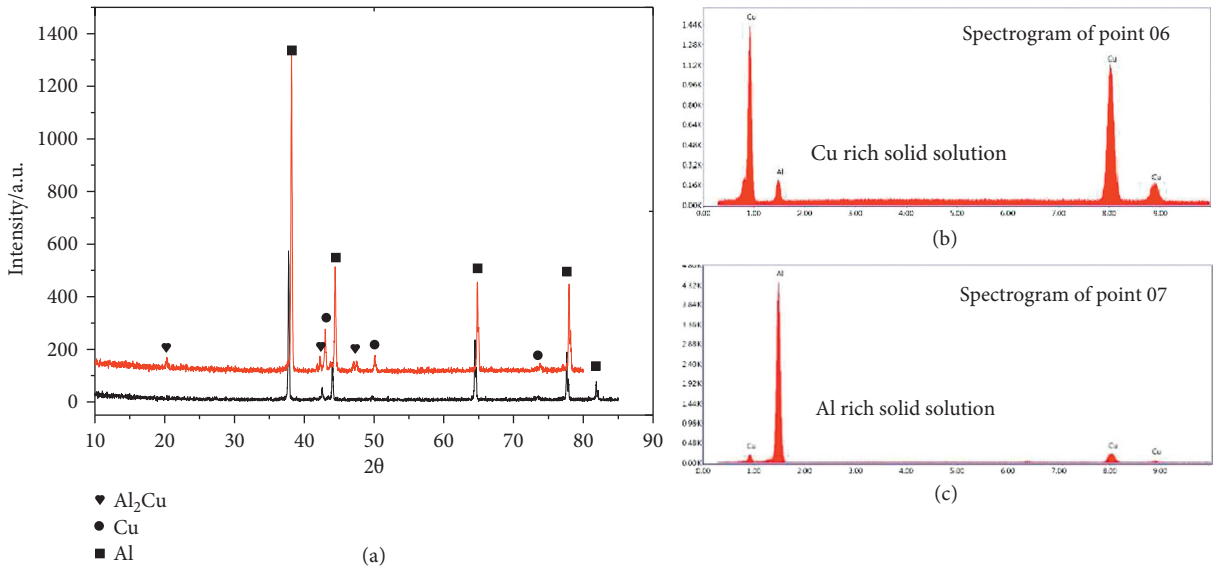

Figure 5: Analysis of phase composition of the joint prepared by FSW. (a) XRD analysis results and (b, c) spectrograms and element contents.

strength test, three samples were prepared for each parameter. The shear strength of different joints is shown in Figure 8(a). The shear strength of the EW and FSW Cu/Al joints was in the range of 95~105 MPa. It was approximately equal to that of the 1060Al metal. The special interlocking interface structures in the EW joint ensured the high joint strength. The formation of a thin, continuous, and uniform diffusion layer was the main reason of the good bonding strength of the FSW joint [27, 28]. The shear strength of the joint prepared by the DB process was approximately 67 MPa. This was mainly due to the stratified structure of the IMCs.

The microhardness distributions were obtained, as shown in Figure 8(b). The microhardness on the Cu/Al interface was much higher than that on the matrix due to the presence of IMCs. It had a high microhardness range of 363–409 HV in the interface area in the EW Cu/Al joints. The width of the high hardness region corresponds to the microstructure analysis of the interface in Figure 6. Only a few points of high microhardness were detected in the transition layer of the DB and FSW Cu/Al joint. That might be because the thickness of the interfacial transition layer was so small that only a few points fell on the IMCs.

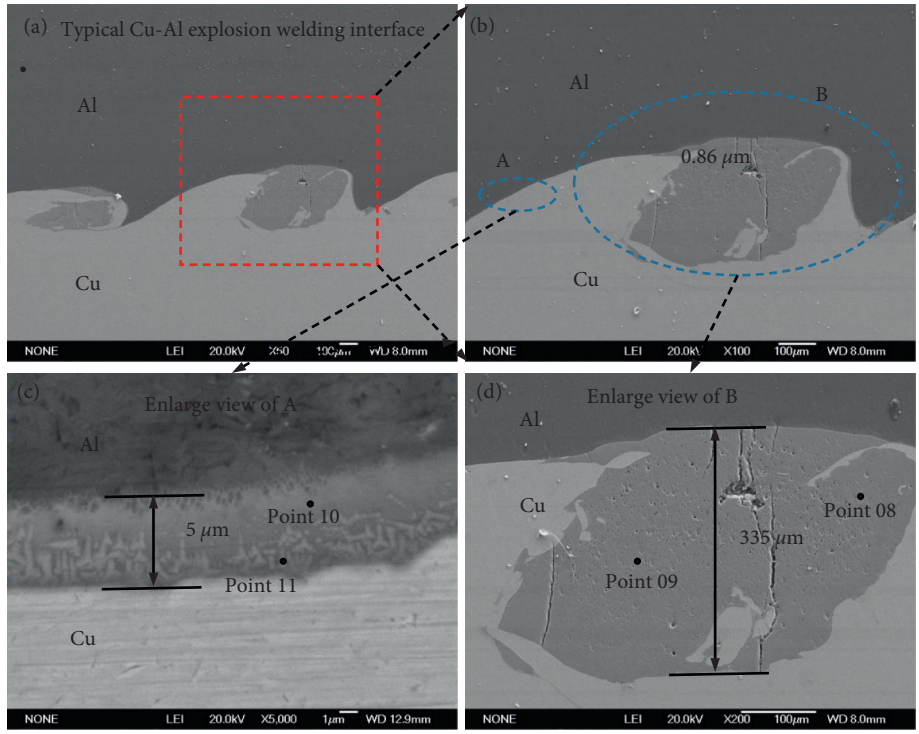

Figure 6: The microstructure of Cu/Al joint produced by EW. (a, b) Interface microstructure, (c) an enlarge view of A, and (d) an enlarge view of B.

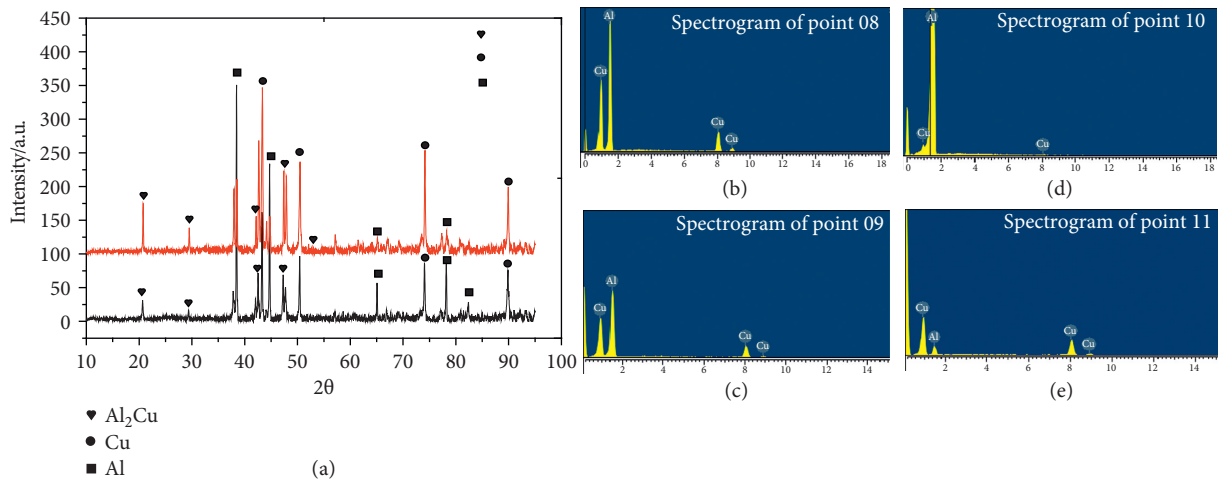

Figure 7: Analysis of phase composition of the joint prepared by explosive welding. (a) XRD analysis results and (b–e) spectrograms and element content of different regions.

3.3. Evaluation of Interfacial Thermal Conductivity Cu-Al Heterogeneous Interface

3.3.1. Thermal Conduction Model of Cu/Al Composite Structure. As a heat conduction component widely used in the field of heat dissipation and refrigeration field (heat dissipation substrates, compressors, etc.), the interfacial thermal conductivity of the Cu/Al structure was an important performance in practical application. The microstructure of the Cu/Al interfacial region, such as the composition and distribution of phases, will have a significant impact on the thermal conductivity of the interface. There has been a lot of research studies on the thermal conductivity of the metal/nonmetal interface. For example, Tan et al. [29] compared the effects of the type and the thickness of the interface transition layer (ITL) on the thermal conductivity of the composite structure. It showed that the thermal conductivity of the composite material decreases as the thickness of the ITL increases. For Cu and Al pure metals on both sides, electron conduction is the main mechanism. For intermetallic compounds, phonon conduction is the main mechanism. Therefore, for the Cu/Al

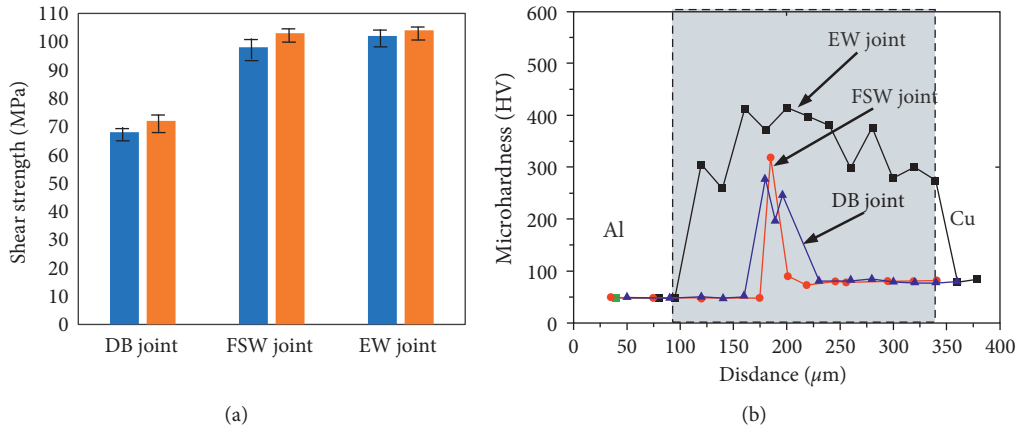

Figure 8: Mechanical properties of three kinds of Cu/Al joints. (a) Shear strength and (b) microhardness distribution.

interfacial region where multiple layers of compounds are generated, not only the thermal conductivity of the compound layer itself but also the thermal conductivity of the metal/compound interface must be considered.

The total interfacial thermal conductivity (h_{total}) of the Cu/Al composite structure can be determined by series total thermal resistance at all surfaces. The calculation principle is the same as that of series resistance in the circuit. The expression is shown as follows [30]:

$$\frac{1}{h_{\text{total}}} = \frac{1}{h_{Al/\text{IMC}}} + \frac{d_{\text{IMC}}}{k_{\text{IMC}}} + \frac{1}{h_{Cu/\text{IMC}}}. \tag{1}$$

Here, $h_{\text{Al/IMC}}$ is the interfacial thermal conductivity between Al and the IMC, k_{IMC} is the thermal conductivity of the IMCs, d_{IMC} is the thickness of the IMC transition layer, and $h_{\text{IMC/Cu}}$ is the interfacial thermal conductivity between Cu and the IMC. When the heat is transferred in the Cu/Al composite structure, the phonon is the main heat transfer medium in the IMC layer, and the electron is the main carrier of the heat transfer in the Cu and Al substrates on both sides. At the interface between the base metal and the IMC interface, the heat is transferred through the phonon-phonon and phonon-electron coupling. The thermal conductivity of the interface can be calculated using the acoustic mismatch model (AMM) as follows [31]:

$$h = \frac{1}{2}\rho_1 \cdot C_p \frac{v_1^3}{v_1^2} \cdot \frac{\rho_1 v_1 \rho_2 v_2}{(\rho_1 v_1 + \rho_2 v_2)^2}. \tag{2}$$

Here, ρ is the material density, C_p is the material-specific heat, and v is the propagation velocity of phonon in a material. When calculating the thermal conductivity at the Al/IMC interface, 1 represents Al and 2 represents IMC. Since the phonon propagation velocity of some materials cannot be obtained from the literature, it can be calculated according to the volume modulus and shear modulus of the material. The specific calculation process is shown as follows:

$$v = \left[\frac{3(v_l v_t)^3}{2v_l^3 + v_t^3}\right]^{1/3},$$
$$v_l = \sqrt{\frac{B + 4/3G}{\rho}}, \tag{3}$$
$$v_t = \sqrt{\frac{G}{\rho}}.$$

Here, the three Cu/Al bonding interfacial regions were analyzed, and the corresponding thermal resistance models were established. In the interfacial region of the DB joint, two layers of IMCs (Al_2Cu and Al_4Cu_9) were formed and distributed in parallel between Al and Cu substrates. The total thermal resistance of the interfacial region was equivalent to the series thermal resistance of each part series, as shown in Figure 9(a). Based on the thermal resistance model, the total interfacial thermal conductivity (h_{total}) can be estimated by the following equation:

$$\frac{1}{h_{\text{total(DB)}}} = \frac{1}{h_{\text{Al/Al}_2\text{Cu}}} + \frac{d_{\text{Al}_2\text{Cu}}}{k_{\text{Al}_2\text{Cu}}} + \frac{1}{h_{\text{Al}_2\text{Cu/Al}_4\text{Cu9}}} + \frac{d_{\text{Al}_4\text{Cu}_9}}{k_{\text{Al}_4\text{Cu}_9}} + \frac{1}{h_{\text{Al/Al}_2\text{Cu}_9}}. \tag{4}$$

The total interfacial thermal conductivity was calculated analytically according to equation (6) and the base data in Table 2, as shown in Figure 9(b). The interfacial thermal conductivity of the DB joint was in the range of $1\sim8\times10^6\,\text{W m}^{-2}\cdot\text{K}^{-1}$ when the thickness of the ITL was in the range of 5~12 μm. When the thickness of the ITL was small, the thermal conductivity decreased rapidly with the increase of the thickness. When the thickness of the ITL was greater than 15 μm, the interfacial thermal conductivity decreased t slowly and tended to a constant value.

For the interfacial region of the FSW joint, a mixture of a supersaturated solid solution and a few dispersed

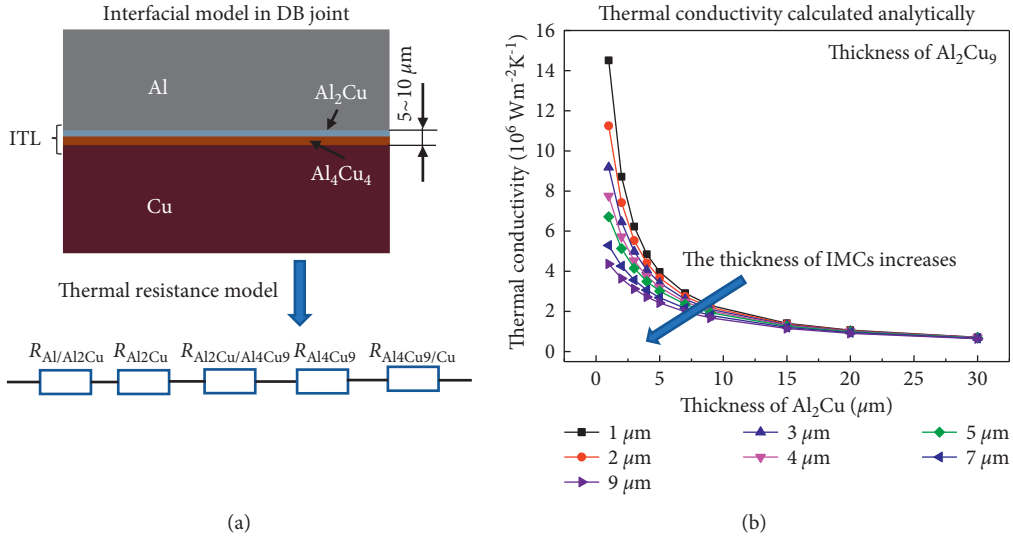

Figure 9: The interfacial thermal resistance model of the joint prepared by DB. (a) The interfacial region and thermal resistance model and (b) interfacial thermal conductivity varying with the thickness of the IMCs.

Table 2: Relevant parameters for the calculation of thermal conductivity.

	KW·m^{-1}·K^{-1}	ρKg·m^{-3}	C$_p$J·kg^{-1}·K^{-1}	GGPa	BGPa	v m·s^{-1}		
						v_t	v_1	$v_{average}$
Al	230	2700	904	26	76	6420	3130	3595
Cu	400	8930	385			2500	4910	2801
Al_2Cu	21.8	4360	500	37.1	99.4	2917	5843	3154
Al_4Cu_9	50	6850	537	63.3	128.0	3040	5568	3236

compounds were distributed between Al and Cu. The total thermal resistance was equivalent to the series thermal resistance of the interfacial layer and the interfaces on both sides, as shown in Figure 10(a). Based on the thermal resistance model, the total interfacial thermal conductivity (h_{total}) of the joint prepared by FSW can be estimated by equation (5). The calculation results of interfacial thermal conductivity according to equation (7) and the base data in Table 2 are shown in Figure 10(b). It can be found that the interfacial thermal conductivity of the FSW joint was in the range of $1\sim25\times10^7$ W m^{-2}·K^{-1}, and the thickness of the ITL was in the range of 0.5~1.5 μm. With the increase of the thickness of the ITL, the interfacial thermal conductivity decreased rapidly and then tended to a constant value. Considering that the ITL is a mixture of a supersaturated solid solution and a few dispersed compounds, different thermal conductivity (k) of the ITL (in the range of 21.8~230 W m^{-1}·K^{-1}) were selected. With the increase of the thermal conductivity (k) of the ITL, the interfacial thermal conductivity increased, as shown in Figure 10(b).

$$\frac{1}{h_{total\,(FSW)}} = \frac{1}{h_{Al/transition\ layer}} + \frac{d_{transition\ layer}}{k_{transition\ layer}} + \frac{1}{h_{Cu/transition\ layer}}. \tag{5}$$

Given the actual interfacial structure of the EW Cu/Al joint in Figure 6(a), the interfacial thermal resistance model can be abstracted, as shown in Figure 11(a). Combined with the actual characteristics of the explosive welding Cu/Al interfacial region, the total thermal resistance can be expressed as the thermal resistance of the narrow interface region and the vortex region in series and then calculated in parallel. The total interfacial thermal conductivity (h_{total}) of the EW joint can be estimated by equation (6). Based on the data in Table 2 and equation (6), the interfacial thermal conductivity was calculated analytically, as shown in Figure 11(b). The interfacial thermal conductivity of the joint prepared by EW was in the range of $1\sim35\times10^5$ W m^{-2}·K^{-1}.

$$h_{(EW)} = \left(h_{Al/solid\ solution} + \frac{k_{solid\ solution}}{d_{solid\ solution}} + h_{Cu/solid\ solution}\right)\times p + \left(h_{Al/Al2cu} + \frac{k_{Al2cu}}{d_{Al2cu}} + h_{Cu/Al2cu}\right)\times(1-p), \tag{6}$$

where p is the ratio of the vortex region.

3.3.2. Experimental Measurements of Thermal Conductivity Cu/Al Joint. The thermal conductivity of the Cu/Al composite structure was determined by the xenon lamp thermal conductivity apparatus Netzsch LFA457 Microflash®. The Cu/Al sample containing the interfacial transition layer is processed into a cylinder with the specification of

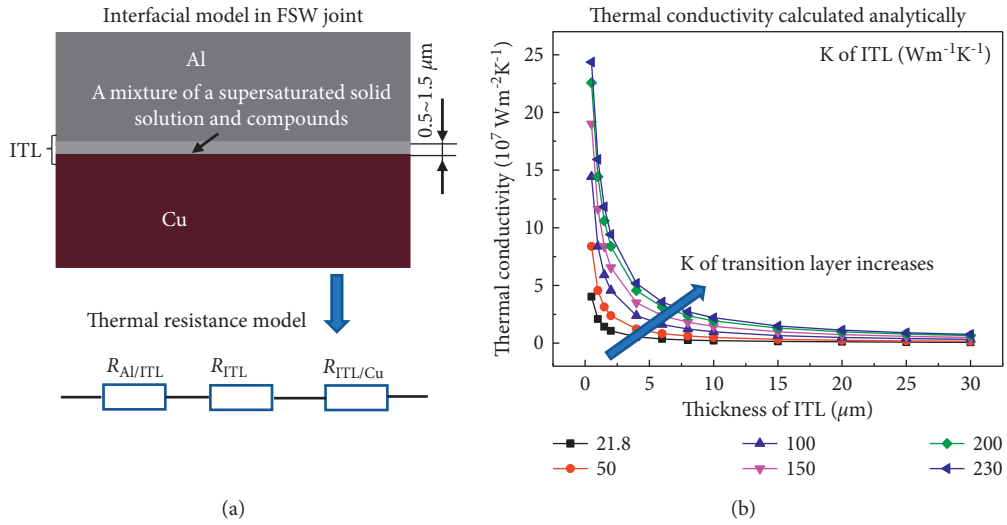

Figure 10: The interfacial thermal resistance model of the joint prepared by FSW. (a) The interfacial region and thermal resistance model and (b) interfacial thermal conductivity varying with the thickness of the IMCs.

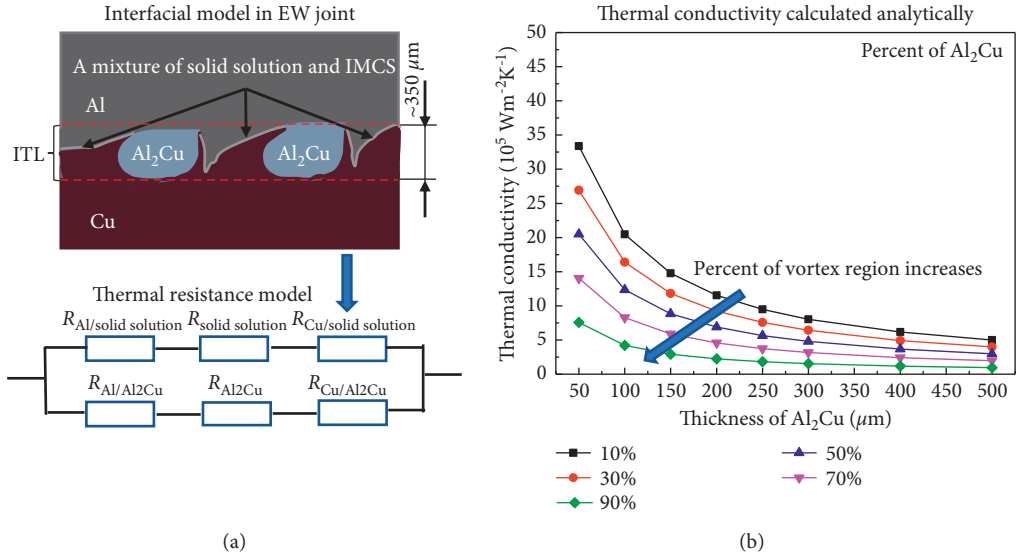

Figure 11: The interfacial thermal resistance model of the joint prepared by EW. (a) The interfacial region and thermal resistance model and (b) interfacial thermal conductivity varies with the thickness of the IMCs.

Ø10 mm × 1 mm. The thermal diffusivity was obtained by the laser flash method under the condition of adiabatic. The thermal conductivity was calculated by the equation as follows:

$$\lambda(T) = \alpha(T) \cdot \rho(T) \cdot C_p(T), \tag{7}$$

where α(T) is the thermal diffusion coefficient, $C_p(T)$ is the specific heat capacity, and $\rho(T)$ is the density. The measured values of thermal conductivity and thermal diffusion coefficient change with temperature are shown in Figure 12. Figures 12(a)–12(c) show the change of thermal diffusion coefficient with the temperature of the interfacial transition layer, aluminum matrix, and copper matrix of three kinds of joints. And Figures 12(d)–12(f) show the corresponding thermal conductivity as a function of temperature. With the increase of temperature, the thermal diffusivity decreases monotonically. The thermal conductivity of joints prepared by DB and FSW was higher than that of the Al base metal, while the thermal conductivity of EW is lower than that of the Al base metal. A comparison of the calculated and experimental values of thermal conductivity is shown in Table 3.

Considering the interfacial microstructure of the different Cu/Al joints, the corresponding interface thermal conductivity model was built. The calculation results show that the interfacial thermal conductivity mainly depends on the type of interfacial phase and its thickness. The structural defects (cracks, cavities, etc.) and IMCs in the joints can seriously affect the interfacial thermal conductivity. Because

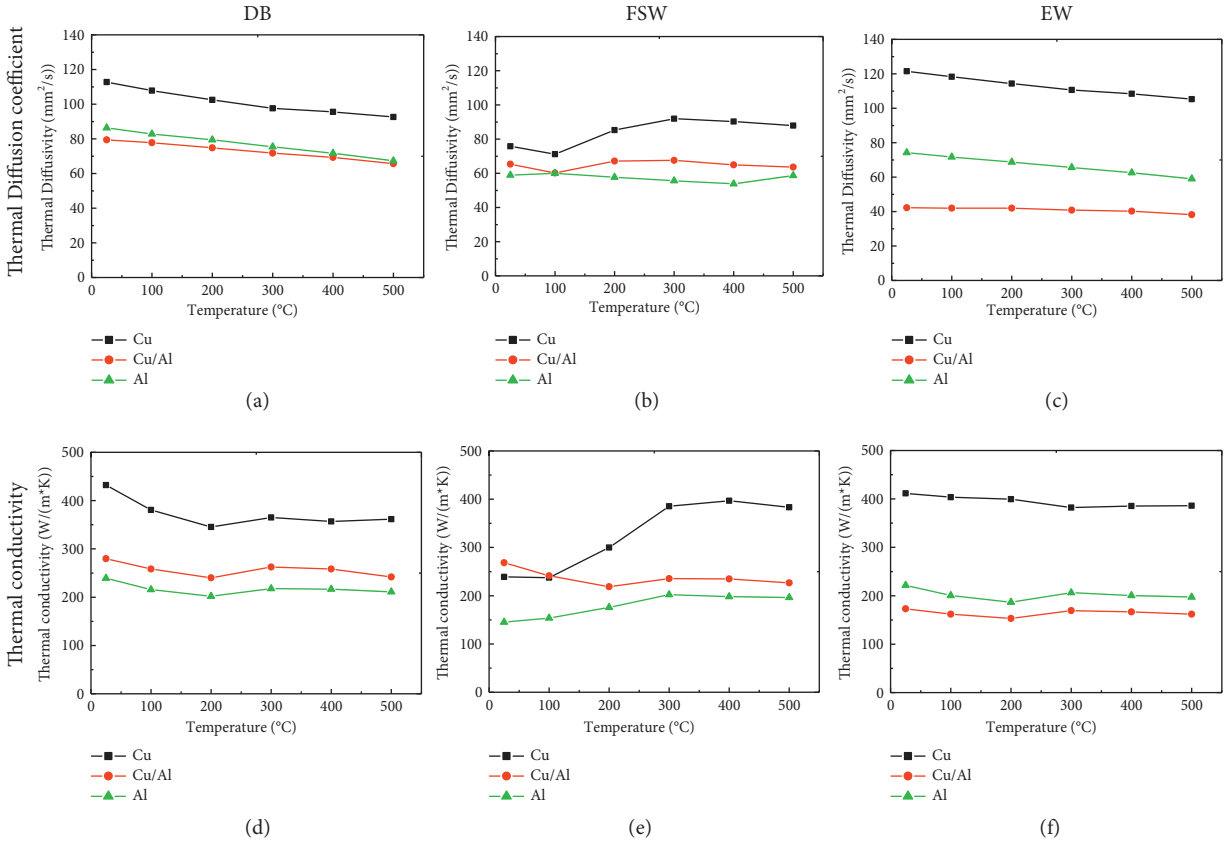

Figure 12: The measured values of thermal conductivity and thermal diffusion coefficient change with temperature.

Table 3: Comparison of the calculated and experimental values of thermal conductivity.

Welding method	The calculated interfacial thermal conductivity ($W{\cdot}m^{-2}{\cdot}K^{-1}$)	Measured thermal conductivity ($W{\cdot}m^{-1}{\cdot}K^{-1}$)
DB	$1\sim8\times10^{6}\,W\,m^{-2}{\cdot}K^{-1}$	250~280
FSW	$1\sim25\times10^{7}\,W\,m^{-2}{\cdot}K^{-1}$	230~270
EW	$1\sim35\times10^{5}\,W\,m^{-2}{\cdot}K^{-1}$	150~180

of the low intrinsic thermal conductivity and the discontinuity of the lattice structure, the hot carriers were heavily scattered, which significantly reduced the interfacial thermal conductivity. The interfacial thermal conductivity of the FSW joint was the highest ($1\sim25\times10^{7}\,W\,m^{-2}{\cdot}K^{-1}$). The calculated interfacial thermal conductivity was compared with the experimental values. The experiments suggest that the interfacial thermal conductivity results preserve the trend that explosive welding < friction stir welding < diffusion bonding. There are two main reasons for the low measured thermal conductivity of FSW joints. One was that some copper particles entered into the aluminum matrix near the interface and formed compounds, which reduces the thermal conductivity. The other is the obvious grain refinement in which the metal near the interface has undergone large plastic deformation and dynamic recrystallization.

4. Conclusion

The main motivation of this paper was to evaluate the effect of interfacial microstructure on the thermal conductivity of the Cu/Al joints prepared by DB, FSW, and EW. The interfacial microstructure and compositions were examined. The thermal conductivity of the three types of joints was estimated, and the corresponding interface thermal conductivity model was built. The main conclusions are as follows:

(1) In the interfacial region of the DB joint, two layers of IMCs (Al_2Cu and Al_4Cu_9) were formed and distributed in parallel between Al and Cu substrates. The total width of the ITL was in the range of 5~12 μm. For the interfacial region of the FSW joint, an obvious diffusion layer (a mixture of a supersaturated solid solution and few dispersed compounds) was formed on the Cu/Al interface with a thickness less than 1 μm. The bonding interface of the Cu/Al EW joint presented a wavy-like morphology. The vortex region consisted of a vortex-like structure with a width of 300~350 μm which consisted a large number of Al_2Cu.

(2) The thermal conductivity was estimated, and the corresponding interface thermal conductivity model was built. The interfacial thermal conductivity with

different interfacial microstructures was calculated analytically using the acoustic mismatch model and compared with the measured value of the joints. The interfacial thermal conductivity mainly depends on the type of interfacial phase and its thickness. The calculated result shows that the interfacial thermal conductivity of the FSW joint was the highest. The experiments results suggested that the interfacial thermal conductivity results preserve the trend that EW < FSW < DB.

Data Availability

The data used to support the findings of this study are included within the article.

Conflicts of Interest

The authors declare no conflicts of interest.

Authors' Contributions

Wei, Chen, and Niu conceptualized the study; Yang and Luo investigated the study; Zou collected the resources; Wei written the original draft.

Acknowledgments

This work was financially supported by the National Natural Science Foundation of China under Grant no. 51701154, the Key Research and Development Project of Shaanxi Province under Grant no. 2018ZDXM-GY-136, and Yunnan Chihong Zn & Ge Co., Ltd Nonferrous Metal Electrodeposition Technology Innovation Team of Yunnan Province (201905E160007).

References

[1] H. Xu, I. Qin, H. Clauberg, B. Chylak, and V. L. Acoff, "New observation of nanoscale interfacial evolution in micro Cu-Al wire bonds by in-situ high resolution TEM study," *Scripta Materialia*, vol. 115, pp. 1–5, 2016.

[2] Y. Wang, R. Song, J. Yanagimoto, and H. Li, "Effect of heat treatment on bonding mechanism and mechanical properties of high strength Cu/Al/Cu clad composite," *Journal of Alloys and Compounds*, vol. 801, pp. 573–580, 2019.

[3] H. G. Kim, M. K. Sang, and J. Y. Lee, "Microstructural evaluation of interfacial intermetallic compounds in Cu wire bonding with Al and Au pads," *Acta Materialia*, vol. 64, pp. 356–366, 2014.

[4] R. Pelzer, M. Nelhiebel, R. Zink, S. Wöhlert, A. Lassnig, and G. Khatibi, "High temperature storage reliability investigation of the Al-Cu wire bond interface," *Microelectronics Reliability*, vol. 52, no. 9-10, pp. 1966–1970, 2012.

[5] S. Dhara and A. Das, "Impact of ultrasonic welding on multi-layered Al-Cu joint for electric vehicle battery applications: a layer-wise microstructural analysis," *Materials Science and Engineering A*, vol. 791, Article ID 139795, 2020.

[6] A. Gueydan, B. Domengès, and E. Hug, "Study of the intermetallic growth in copper-clad aluminum wires after thermal aging," *Intermetallics*, vol. 50, pp. 34–42, 2014.

[7] W.-B. Lee, K.-S. Bang, and S.-B. Jung, "Effects of intermetallic compound on the electrical and mechanical properties of friction welded Cu/Al bimetallic joints during annealing," *Journal of Alloys and Compounds*, vol. 390, no. 1-2, pp. 212–219, 2005.

[8] M. Akbari, P. Bahemmat, M. Haghpanahi, and M.-K. Besharati Givi, "Enhancing metallurgical and mechanical properties of friction stir lap welding of Al-Cu using intermediate layer," *Science and Technology of Welding and Joining*, vol. 18, no. 6, pp. 518–524, 2013.

[9] X. Zhang, Y. Yu, B. Liu, and J. Ren, "Mechanical properties and tensile fracture mechanism investigation of Al/Cu/Ti/Cu/Al laminated composites fabricated by rolling," *Journal of Alloys and Compounds*, vol. 805, pp. 338–345, 2019.

[10] J. Xiong, Y. Peng, H. Zhang, J. Li, and F. Zhang, "Microstructure and mechanical properties of Al-Cu joints diffusion-bonded with Ni or Ag interlayer," *Vacuum*, vol. 147, pp. 187–193, 2018.

[11] Z. Niu, Z. Ye, J. Huang, H. Yang, J. Yang, and S. Chen, "Interfacial structure and properties of Cu/Al joints brazed with Zn-Al filler metals," *Materials Characterization*, vol. 138, pp. 78–88, 2018.

[12] H. Yu, L. Zhang, F. Cai et al., "Interface microstructure and growth mechanism of brazing Cu/Al joint with BAl88Si filler metal," *Vacuum*, vol. 181, Article ID 109641, 2020.

[13] W. Hou, L. H. Ahmad Shah, G. Huang, Y. Shen, and A. Gerlich, "The role of tool offset on the microstructure and mechanical properties of Al/Cu friction stir welded joints," *Journal of Alloys and Compounds*, vol. 825, Article ID 154045, 2020.

[14] Y. Wei, F. Sun, H. Li, X. Peng, and J. Zou, "The microstructure and mechanical properties of multipass friction stir-welded Al/Cu lap joints and interface transfer during butt joining of thick plates," *Advanced Engineering Materials*, vol. 22, no. 11, Article ID 2000346, 2020.

[15] Y. N. Wei, H. Li, X. Peng, and J. T. Zou, "Microstructure and conductivity of the Al-Cu joint processed by friction stir welding," *Advances in Materials Science and Engineering*, vol. 2020, Article ID 6845468, 10 pages, 2020.

[16] W.-S. Shin, D.-W. Cho, D. Jung et al., "Investigation on laser welding of Al ribbon to Cu sheet: weldability, microstructure, and mechanical and electrical properties," *Metals*, vol. 11, no. 5, p. 831, 2021.

[17] M. Honarpisheh, M. Asemabadi, and M. Sedighi, "Investigation of annealing treatment on the interfacial properties of explosive-welded Al/Cu/Al multilayer," *Materials & Design*, vol. 37, pp. 122–127, 2012.

[18] Y. N. Wei, Y. G. Luo, H. T. Qu, J. T. Zou, and S. H. Liang, "Microstructure evolution and failure analysis of an aluminum-copper cathode conductive head produced by explosive welding," *Journal of Materials Engineering and Performance*, vol. 26, pp. 1–9, 2017.

[19] C.-Y. Chen, H.-L. Chen, and W.-S. Hwang, "Influence of interfacial structure development on the fracture mechanism and bond strength of aluminum/copper bimetal plate," *Materials Transactions*, vol. 47, no. 4, pp. 1232–1239, 2006.

[20] X.-G. Wang, X.-G. Li, and C.-G. Wang, "Influence of diffusion brazing parameters on microstructure and properties of Cu/Al joints," *Journal of Manufacturing Processes*, vol. 35, pp. 343–350, 2018.

[21] S. Tavassoli, M. Abbasi, and R. Tahavvori, "Controlling of IMCs layers formation sequence, bond strength and electrical resistance in Al Cu bimetal compound casting process," *Materials & Design*, vol. 108, pp. 343–353, 2016.

[22] Y. Tanaka, M. Kajihara, and Y. Watanabe, "Growth behavior of compound layers during reactive diffusion between solid Cu and liquid Al," *Materials Science and Engineering A*, vol. 445–446, pp. 355–363, 2007.

[23] N. A. Muhammad and C. Wu, "Evaluation of capabilities of ultrasonic vibration on the surface, electrical and mechanical behaviours of aluminium to copper dissimilar friction stir welds," *International Journal of Mechanical Sciences*, vol. 183, Article ID 105784, 2020.

[24] H. Bisadi, A. Tavakoli, M. Tour Sangsaraki, and K. Tour Sangsaraki, "The influences of rotational and welding speeds on microstructures and mechanical properties of friction stir welded Al5083 and commercially pure copper sheets lap joints," *Materials & Design*, vol. 43, pp. 80–88, 2013.

[25] Y. Wei, F. Sun, S. Tan, and S. Liang, "Study on microstructure and performance of transient liquid phase bonding of Cu/Al with Al-based interlayers," *Vacuum*, vol. 154, pp. 18–24, 2018.

[26] Y. N. Wei, H. Li, F. Sun, and J. T. Zou, "The interfacial characterization and performance of Cu/Al conductive heads processed by explosion welding, cold pressure welding, and solid-liquid casting," *Metals*, vol. 9, no. 237, pp. 1–13, 2019.

[27] M. Abbasi, A. Karimi Taheri, and M. T. Salehi, "Growth rate of intermetallic compounds in Al/Cu bimetal produced by cold roll welding process," *Journal of Alloys and Compounds*, vol. 319, no. 1-2, pp. 233–241, 2001.

[28] P. Xue, B. L. Xiao, D. R. Ni, and Z. Y. Ma, "Enhanced mechanical properties of friction stir welded dissimilar Al–Cu joint by intermetallic compounds," *Materials Science and Engineering A*, vol. 527, no. 21-22, pp. 5723–5727, 2010.

[29] Z. Tan, Z. Li, G. Fan et al., "Enhanced thermal conductivity in diamond/aluminum composites with a tungsten interface nanolayer," *Materials & Design*, vol. 47, pp. 160–166, 2013.

[30] Y. Zhang, H. L. Zhang, J. H. Wu, and X. T. Wang, "Enhanced thermal conductivity in copper matrix composites reinforced with titanium-coated diamond particles," *Scripta Materialia*, vol. 65, no. 12, pp. 1097–1100, 2011.

[31] J. M. Molina, R. Prieto, J. Narciso, and E. Louis, "The effect of porosity on the thermal conductivity of Al–12wt.% Si/Si C composites," *Scripta Materialia*, vol. 60, no. 7, pp. 582–585, 2009.